Available online at www.sciencedirect.com

SciVerse ScienceDirect

Ceramics International 39 (2013) 1065–1073

CERAMICS INTERNATIONAL

www.elsevier.com/locate/ceramint

Application of hydrophilic ionic liquid treatment to the morphological observations of hydrated porous ceramic green bodies

Chisato Takahashi[a], Deepak K. Pattanayak[a,b], Takashi Shirai[a], Masayoshi Fuji[a,*]

[a]*Advanced Ceramics Research Center, Nagoya Institute of Technology, 3-101-1 Honmachi, Tajimi, Gifu 507-0033, Japan*
[b]*CSIR-Central Electrochemical Research Institute, Karaikudi, Tamilnadu 630006, India*

Received 4 June 2012; received in revised form 6 July 2012; accepted 7 July 2012
Available online 21 July 2012

Abstract

In this study, a simple and convenient method for observing the surface morphology of hydrated porous ceramic green bodies is proposed. The porous hyrdoxyapatite (HAp) green body was prepared by a gelcasting process and was dried in a humid chamber from 90 to 50% relative humidity at 25 °C before subsequent treatment with a hydrophilic ionic liquid (IL). The surface morphology of the IL-treated porous HAp green body was observed using FE-SEM. The results showed that the pore morphology and microstructure of the HAp green body was readily observable without evidence of charging. The as-prepared sample showed pores approximately 300–600 μm in diameter, which gradually contracted to approximately 200–400 μm upon drying in the humid chamber. Following sintering at 1000 °C, the pores had further contracted to approximately 100–300 μm. The IL binds with the surrounding water to prevent the sample from drying in vacuum and acts as a conductive media, allowing the HAp ceramics to be observed in the electron microscope. In comparison to the micro-focused X-ray CT analysis, the fine pore structure (less than 100 μm) could only be observed using FE-SEM when the porous body had also been subjected to the IL treatment.

Keywords: Ionic liquid; Gelcasting; Hydrated materials; FE-SEM

1. Introduction

Among the various types of calcium phosphate ceramics, hydroxyapatite [$Ca_{10}(PO_4)_6(OH)_2$, HAp] is a well-known biocompatible material and is naturally found as one of the major components of bone and tooth [1–4]. As-synthesised HAp ceramics show both osteoconductivity and osteoinductivity and directly bonds to living bone through the native apatite phase [5,6]. However, for enhanced bone integration and mechanical interlocking between implanted devices and the newly grown bone tissues, particular attention must be paid to the processing of the porous HAp body [7].

A variety of methods for fabricating porous HAp bodies have been described in the literature; these include the impregnation of polymeric sponges, gelcasting of foam, extrusion and other automated manufacturing methods [8–11]. Among these methods, gelcasting, which was developed by Janney et al., can be used to fabricate samples with complex shapes and high mechanical strength [12,13]. This method also has been successfully applied to other ceramics, such as alumina [14–16], silicon nitride [17], rutile [18], silicon carbide [19,20], and alumina–zirconia composites [21,22]. Additionally, following the solidification step, when this method is further combined with foamed suspensions by in situ polymerisation, it can be used to form an internally cross-linked network, that transforms the foam into a gelled body with the ability to bear load [23–26]. The gelled body is then sintered to create the final material, which can be used in various functional applications. Although several researchers have used scanning electron microscope (SEM) to describe the surface morphology and the microstructure of gelcast porous ceramics in either the dried or sintered conditions, there

*Corresponding author. Tel.: +81 572 24 8110; fax: +81 572 24 8109.
E-mail address: fuji@nitech.ac.jp (M. Fuji).

0272-8842/$ - see front matter © 2012 Elsevier Ltd and Techna Group S.r.l. All rights reserved.
http://dx.doi.org/10.1016/j.ceramint.2012.07.028

have been no reports that describes the microstructure of the green body in its hydrated condition immediately following fabrication. This is because the water-containing ceramic materials present certain limitations for SEM observations, which necessitate the use of vacuum conditions in the microscope chamber. However, to establish enhanced processing conditions for ceramics, it is necessary to understand the complex structure of the green body. Thus, it is essential to develop new techniques for microscopic observations of ceramic bodies in the hydrated form.

Recently, room-temperature (RT) ionic liquids (ILs) have attracted significant attention as novel, eco-friendly materials that can be used as solvents in inorganic chemistry, electrochemistry, catalysis, etc [27–29]. These ILs are composed of cations and anions, which exist in a liquid state at RT. Due to their negligible vapour pressure and high conductivity, various studies have also revealed that combinations of ILs with samples can be directly observed in the electron microscope without the addition of a conductive coating [30–32]. Some reports have further suggested that hydrated materials, such as seaweed and chicken tissue are observable by SEM when mixed with hydrophilic ILs [33,34]. The author of this study has previously reported that hydrated agar gel can be successfully observed using the hydrophilic IL; additionally, a mechanism was proposed for the field emission scanning electron microscope (FE-SEM) observation of gel-type materials that have not been dried in a vacuum chamber [35,36].

In the present study, with the aid of hydrophilic ionic liquid, we observed the surface morphology of the porous HAp green body in its wet condition and compared the changes in pore structure that occur during drying and after sintering. Finally, we propose a general principle for the morphological observation of wet ceramic materials.

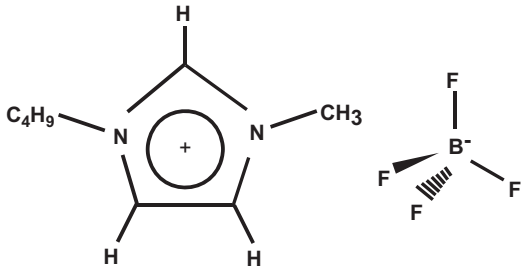

Fig. 1. Chemical structure of the IL used in the present study.

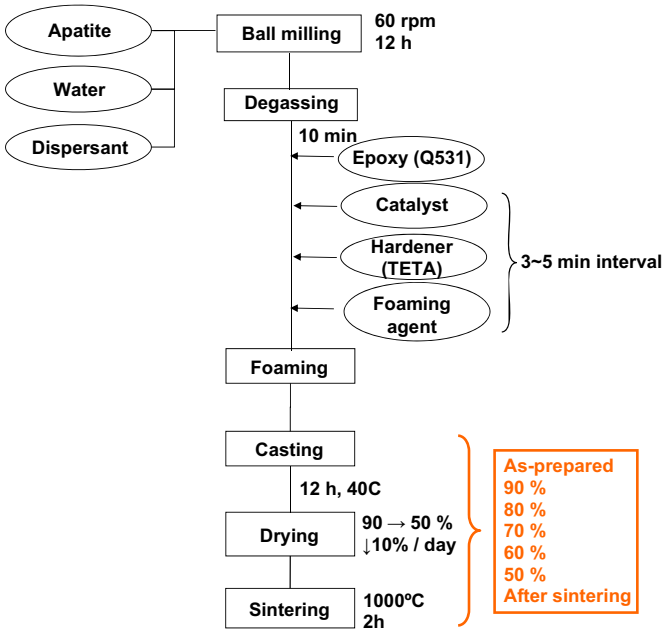

Fig. 2. Schematic representation of the gelcasting process used in the present study.

2. Materials and methods

A hydroxyapatite (HAp) powder, a dispersant, a monomer and various initiators were used for the gelcasting process. The HAp powder was supplied by Taihei Chem. Co., Japan, with a particle size less than 5 μm. A commercial ammonium salt of polycarboxylate (Seruna D-305) supplied by CHUKYO YUSHI Co., LTD, Japan was used as the dispersant. The organic components (i.e., the epoxy and the hardener) were supplied by CHUKYO YUSHI Co., LTD, Japan, and TETA (Kanto Chemical Co., Japan) was used as the catalyst.

The ionic liquid of choice for analyses was 1-butyl-3-methylimidazolium tetrafluoroborate ((BMIM)(BF_4)) (Kanto Chem. Co., Japan); in all instances, this chemical was dried in a vacuum desiccators at 60 °C for 3 day before use. The chemical structure of the IL is shown in Fig. 1. The water content of the IL was below 128 ppm, as measured by the Karl Fischer titration method.

Fig. 2 shows a schematic representation of the gelcasting process used in this investigation. In the first step, a 40-vol-% slurry was prepared from the HAp powder, water and dispersant by ball milling inside a polyethylene container with zirconia balls for approximately 24 h. The slurry was screen-filtered to remove the zirconia balls and was then degassed for 10 min to remove any trapped air bubbles. The degassed slurry was combined with the epoxy resin, the initiator and the catalyst to initiate the polymerisation process. To incorporate pores into the microstructure, 0.3 g of surfactant (per 100 mL of slurry) were added and mixed with a hand mixer. Finally, the resulting slurry mixture was poured into a rectangular shape mould and was allowed to gel overnight at 40 °C in air. The mould was removed from the freshly gelled body; the specimen was then cut to a size of $5.0 \times 5.0 \times 5.0\ mm^3$ around the central region of the rectangular sample. The trimmed specimens were kept in a humidity-controlled drying chamber at 25 °C for 5 day in such a way that the humidity was reduced from 90 to 50% at a rate of 10% per day.

The water contents of both the as-prepared porous HAp green body and the specimens that had been stored in the

humid chamber were measured by Karl Fischer titration. All porous bodies were cut into the same $5.0 \times 5.0 \times 5.0$ mm^3 in size for this measurement.

The as-prepared samples and the samples stored in the humid chamber were both treated with the IL. The IL was prepared by adjusting its water content to 30 mol% (weight amount ratio; water: IL = 1:29.3) and was stored in a desiccator for 2 h. All these samples were subsequently maintained in a vacuum dryer for 24 h before being centrifugated for 5 min at 10,000 rpm to remove any excess IL. The microstructures of the IL-treated samples were observed using field emission scanning electron microscopy (FE-SEM, JEOL Co., Japan) performed at 5 kV. Additionally, the porous HAp bodies were sintered at 1000 °C for 2 h and were then coated with either conventional osmium metal or the IL solution; the surface morphologies of both cases were compared under FE-SEM. The sintering of the porous bodies was carried out at 1000 °C for 2 h in an atmospheric furnace and the rate of heating was maintained at 1 °C/min to avoid thermal cracking.

The X-ray diffraction (XRD) pattern (Ultima 5, Rigaku Co., Japan) of the hydroxyapatite powder was recorded in the 2θ range from 10 to 60 °C with a scan rate of 1 °C/ min using Cu Kα radiation ($\lambda = 0.1542$ nm, 40 kV, 40 mA). Micro-focused X-ray CT analysis (SMX-90CT, Shimadzu Co., Japan) of the porous HAp green bodies was performed to examine the pore morphology with respect to the drying procedure, and the results were compared to the FE-SEM images, which were collected under similar conditions. Each porous HAp green body was cut into a size of $2.0 \times 2.0 \times 0.5$ cm^3 for this measurement.

The size retention of the as-prepared porous HAp green bodies, the samples that were treated in the humid chamber as it was reduced from 80 to 50% relative humidity, and those that were sintered at 1000 °C for 2 h were all measured both before and after the IL treatment. The dimensions of the samples were measured using a ruler as shown in Fig. S1. The size retention ratios were calculated ($X \times Y \times Z/125 \times 100$).

The pore diameters of the green HAp bodies just following removal from the mould and of those maintained in the humid chamber as it was reduced from 90 to 50% relative humidity were determined from the FE-SEM images. The measurements were taken from an area of 3.0×3.0 mm^2 which was imaged with FE-SEM images and the average pore diameters were calculated from the micrographs of these regions. The diameter of each pore was measured as $X + Y/2$ (Fig. S2). For the pore size distribution measurement, area of 3.0×3.0 mm^2 was recorded both by micro-focused X-ray CT and by FE-SEM imaging; the pore diameters were measured for pores in the range of 50 to 700 μm.

3. Results and discussions

Fig. 3a and b shows the FE-SEM images and XRD spectrum of the as-received HAp powder, respectively. Agglomerated spherical HAp particles of approximately 5–10 μm in diameter can be seen in Fig. 3a; additionally, it can be seen that these grains are composed of approximately 200–400 nm sub-grains (inset Fig. 3a). Further inspection of the XRD pattern indicates that the powder contains a pure HAp phase, identified by the corresponding 2θ values, as shown in Fig. 3b. The HAp powder was subsequently used for the gelcasting process, which was employed to fabricate the porous HAp green body samples.

Fig. 4 shows a comparison of the FE-SEM images of the sintered porous HAp body following either an osmium coating treatment (Fig. 4a–d) or a separate subjection of the porous HAp body to the IL treatment (Fig. 4e–g). It can be seen in the low-magnification image that the sintered sample consists of pores in the range of approximately 100–300 μm in diameter (Fig. 4a). The high-magnification image demonstrates that the porous body consists of HAp particles; the particles have bonded to each other creating nanoporosity between them (Fig. 4b–d). This result indicates the presence of neck formation and of partial sintering among the HAp particles, which were treated at 1000 °C. Additionally, there were no identifiable differences between the FE-SEM images of the samples coated with the osmium metal (Fig. 4a–d), which is a conventional conductive coating used for ceramics

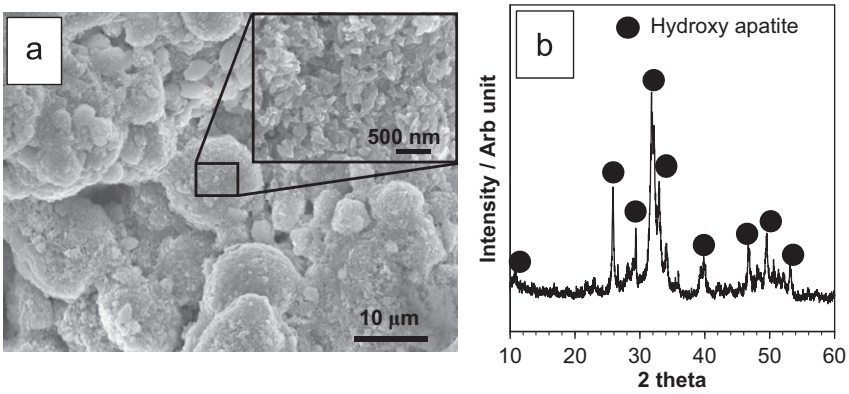

Fig. 3. (a) FE-SEM images of the as-received hydroxyapatite powder, in which the inset shows a high-magnification image, and (b) the corresponding XRD spectrum. All XRD peaks correspond to the structure of hydroxyapatite.

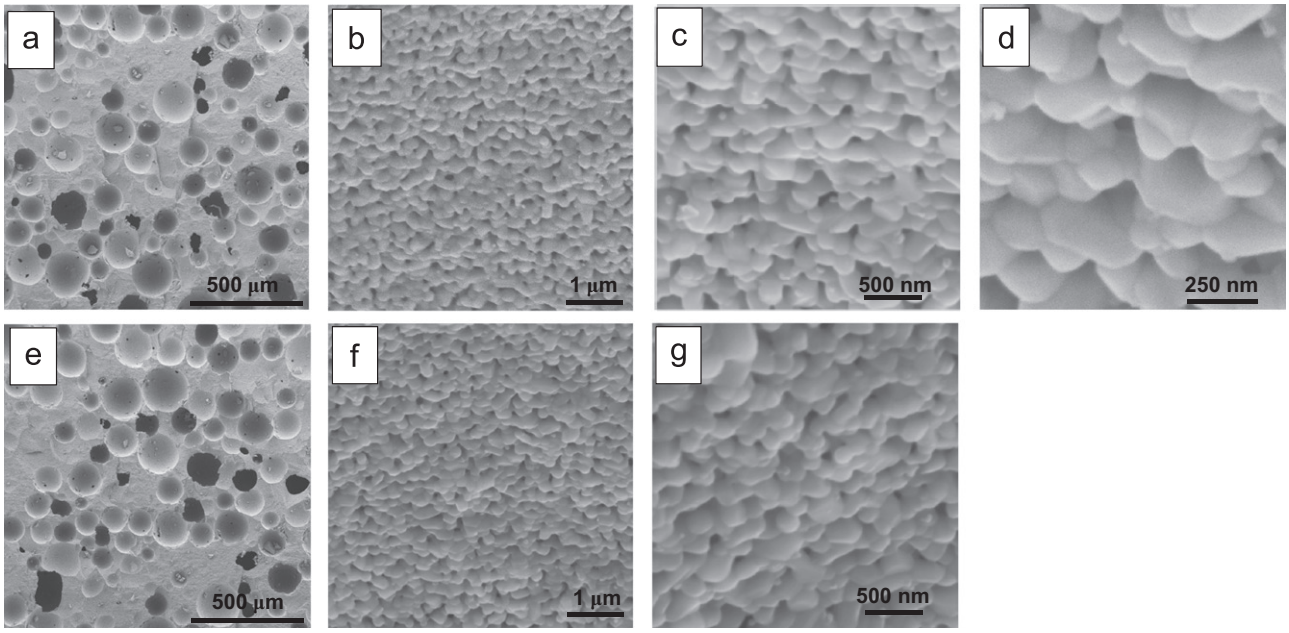

Fig. 4. Comparison of the FE-SEM images of the porous HAp body sintered at 1000 °C for 2 h, following (a)–(d) osmium coating and (e)–(g) the IL treatment. The surface morphologies appeared to be similar for both the osmium-coated and the IL-treated samples.

versus the samples treated with the IL solution (Fig. 4e–g); in both cases no surface-charging was observed despite the high-vacuum conditions within the microscope chamber. This finding indicates that the hydrophilic IL used in this study served a similar purpose as that of the conductive osmium coating; additionally, the IL treatment did not change the surface morphology of the specimen. It has been previously reported that metals or ceramics in dehydrated conditions can be observed using IL solutions [30,32,37]. The present results are in strong agreement with these earlier reports. However, it was not possible to observe the porous HAp body treated with the IL at a very high magnification, which was otherwise achieved for the samples with the osmium coatings, as shown in Fig. 4d. At very high magnifications, the electron beam locally irradiates the porous HAp body and the IL; thus, the IL within the porous body was identified on the sample surface. From this observation, it was determined that the structure of the porous HAp body had significantly changed. From the above results, it was possible to identify the observational limitation associated with the IL treatment. Although the surface morphology of the dried porous HAp body was clearly identifiable for the samples that were treated with the hydrophilic IL, nonetheless, it is interesting to examine the hydrated green body following the same treatment.

Fig. 5a–f shows FE-SEM images of the as-prepared porous HAp green bodies and of the samples that were treated in the humid chamber as it was gradually reduced from 90 to 50% relative humidity by 10% per day; the IL treatment followed this treatment. Fig. 6 shows the high-magnification FE-SEM images of both sample types, the as-prepared and the dehumidified, in similar conditions. It can be seen from Figs. 5 and 6 that the as-prepared porous HAp green body consisted of large pores approximately 300–600 μm in diameter and that, during the course of drying in the humid chamber, the pore size gradually decreased to approximately 200–400 μm.

Table 1 shows the water content both of the porous HAp green bodies immediately following their removal from the mould and of those maintained in the humid chamber as it reduced from 90 to 50% relative humidity. It can be seen in Table 1 that the water content of the as-prepared porous HAp green body was 31.51 wt%; this value gradually decreased as the samples were maintained in the humid chamber. The water content of the samples dried at 50% relative humidity was 11.06 wt%, which indicates that the sample still contained some water. This water was likely to be trapped in the pores as well as within the network structure, which was formed by the polymer and the HAp ceramic. As the trapped water inside the as-prepared green HAp body gradually evaporates inside the humid chamber, a gradual shrinking of the pores and the HAp particles in the polymer network is expected; this phenomenon was observed in Figs. 5 and 6. Further, it can be seen that the green body dried at 50% relative humidity had larger pore sizes than the sample sintered at 1000 °C for 2 h (Figs. 4e and 5f). This result indicates that the remaining trapped water inside the pores and in the networks was evaporated above 100 °C in the electric furnace. Additionally, sintering of the HAp particles at 1000 °C initiated a significant contraction of the pore sizes as the water was evaporated and the polymer was burned out (above 500 °C). Hence, in a comparison of FE-SEM images in Figs. 4 to 6, the morphologies of both the green and the sintered porous HAp bodies are readily observed, even when the samples were subjected to the hydrophilic IL solution without the

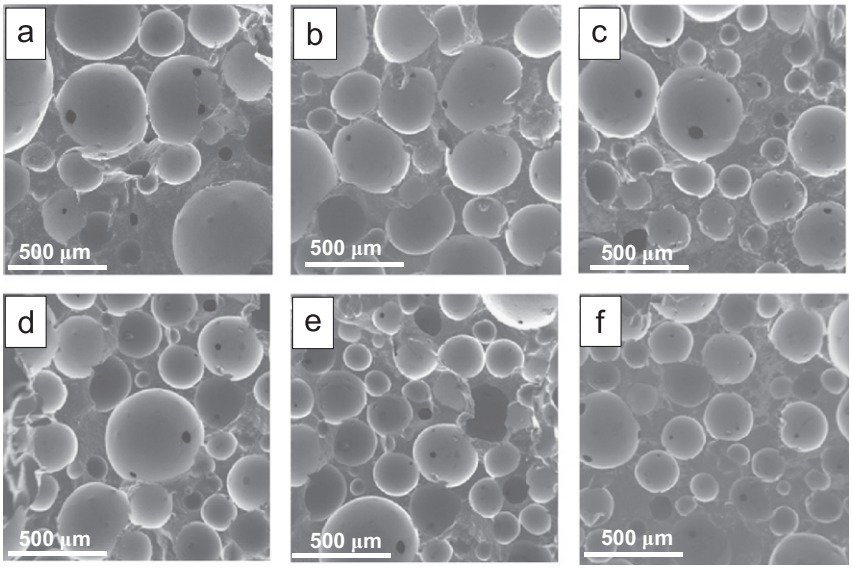

Fig. 5. FE-SEM images of (a) the as-prepared porous HAp green body just after removal from the mould and of the specimens treated in the humid chamber at (b) 90, (c) 80, (d) 70, (e) 60 and (f) 50% relative humidity.

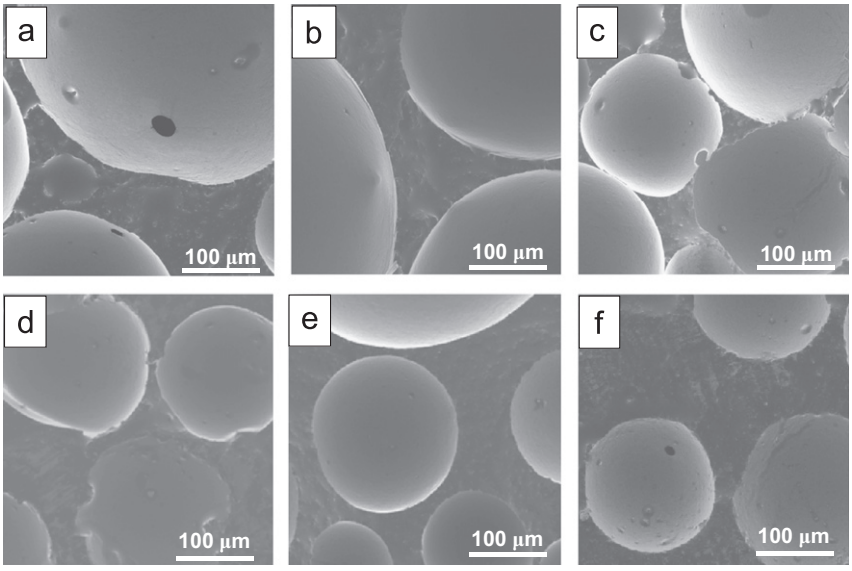

Fig. 6. High-magnification FE-SEM images of (a) the as-prepared porous HAp green body just after removal from the mould and of the specimens treated in the humid chamber at (b) 90, (c) 80, (d) 70, (e) 60 and (f) 50% relative humidity.

Table 1
Comparison of the water contents of the porous HAp green bodies just after removal from the mould and of the samples maintained in the humid chamber as it was reduced from 90 to 50% relative humidity.

Condition	As-prepared	90%	80%	70%	60%	50%
Water content (Wt %)	31.51	25.39	21.25	18.58	15.08	11.06

addition of a conventional conductive coating such as Au, Os, Pt/Pd or carbon. Furthermore, the green body which contains a large amount of water, was readily observed in the FE-SEM chamber under high-vacuum conditions without any drying of samples. The possible reasons for this observation will be discussed later in this section.

Table 2 shows the average pore diameter as measured from the FE-SEM images of the samples with respect to drying and subsequent sintering at 1000 °C for 2 h. From Table 2, it can be seen that the as-prepared porous HAp green body contains pores with an average pore diameter of 342 μm. These pores were gradually reduced in size to approximately 252 μm when the samples were kept in the humid chamber at 50% relative humidity. There is also a possibility that any pores below 100 μm in size might have disappeared during the drying and subsequent sintering processing steps. The porous bodies sintered at 1000 °C for 2 h showed pores with an average diameter of 196 μm.

Fig. 7a–f shows the micro-focused X-ray CT images of both the as-prepared green HAp porous body and the samples

treated in the humid chamber at different humidity values. It can be seen that the as-prepared sample had large pores measuring approximately 300–600 μm (Fig. 7a) and that during the course of drying in the humid chamber, there was a gradual reduction in the pore sizes to approximately 200–400 μm (Fig. 7f). Thus, the observed changes in the pore sizes with respect to the drying condition based on the micro-focused X-ray CT images (Fig. 7) have strong agreement with the FE-SEM images (Fig. 5). In general, the micro-focused X-ray CT technique is useful for generating real images without structural disorder. However, it is difficult to obtain high-magnification or high-resolution images using this method.

Fig. 8a and b shows a comparative study of the distribution of the pore diameters of the porous HAp green body and the samples maintained in the humid chamber, as measured from the micro-focused X-ray CT and FE-SEM images, respectively. Fig. 8a shows that each distribution was shifted during the drying treatment. However, using the micro-focused X-ray CT, any pore sizes below 100 μm could not be observed in either the as-prepared porous body or in the specimens maintained in the humid chamber. Hence, observations of the pore structure using the micro-focused X-ray CT technique were likely limited due to the water contents of the samples. However, it was possible to observe the fine pore structure (below 100 μm in size) with the FE-SEM, and in so doing, a similar trend in the peak shift with respect to the drying condition was noticed (Fig. 8b). Fig. 9 shows the distribution of the average of pore diameters as measured from the micro-focused X-ray CT and FE-SEM images. In particular, the pore diameter of the as-prepared HAp porous green bodies, which possessed a large amount of water, and of the samples maintained in the 90% relative humidity condition were different, according to the results of the micro-focused X-ray CT and FE-SEM images. It is likely that small pores cannot be detected with the micro-focused X-ray CT technique. Therefore, there is the possibility of error in any pore size measurements that are based on this approach.

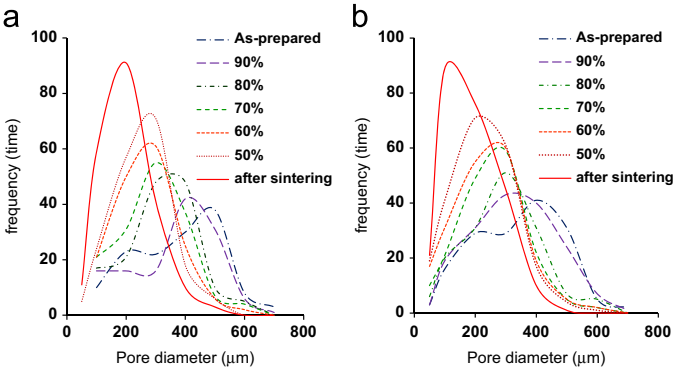

Fig. 8. Comparative study of the distribution of the pore diameters of the porous HAp green body and of the specimens maintained in the humid chamber as it was reduced from 90 to 50% relative humidity; the pore diameter values were measured from (a) the micro-focused X-ray CT and (b) the FE-SEM images.

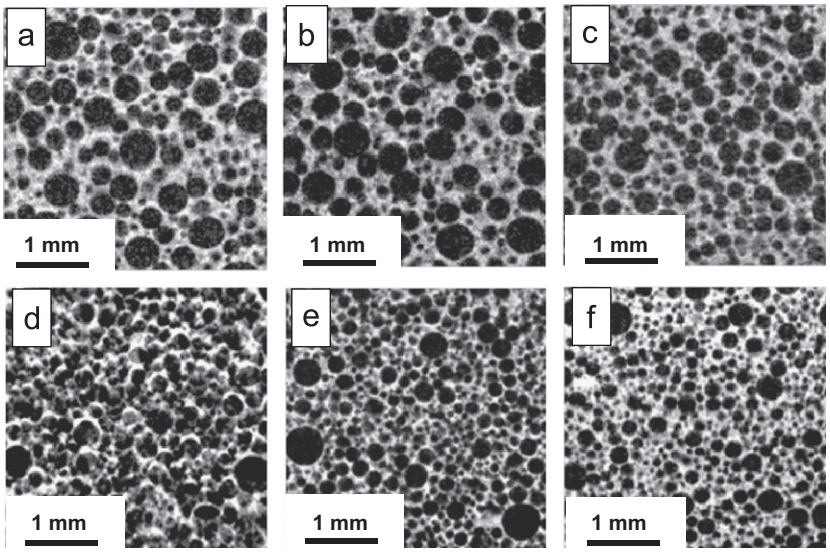

Fig. 7. Micro-focused X-ray CT images of (a) the as-prepared porous HAp green body just after removal from the mould and of the specimens treated in the humid chamber at (b) 90, (c) 80, (d) 70, (e) 60 and (f) 50% relative humidity.

Table 2
Comparison of the change in pore diameter of the porous HAp green bodies just after removal from the mould and of the samples maintained in the humid chamber as it was reduced from 90 to 50% relative humidity.

Condition	As-prepared hydrated green body	90%	80%	70%	60%	50%	After sintering, 1000 °C for 2 h
Average pore diameter (μm)	342	324	299	279	265	252	196

Table 3 shows the dimensional changes in the as-prepared porous HAp green bodies and in the samples that were maintained in the humid chamber at 80 and 50% relative humidity, both of which were followed by sintering at 1000 °C for 2 h before and after the IL treatment. In Table 3, we can see that the porous HAp green body showed significant dimensional changes, i.e., the porosity was 78.6% during drying and 52.7% after sintering at 1000 °C for 2 h. However, when treated under similar conditions and followed by the IL treatment, exhibited only 0.02% shrinkage, which is significantly less. This result indicates that when the porous bodies in different hydrated conditions were subjected to the hydrophilic IL treatment, they further retained their structures without any changes in morphology and with only negligible changes in dimensions. Table 3 shows that approximately 20% volume shrinkage occurs during the course of drying the green HAp porous bodies. In comparing Tables 1 and 3, it can be seen that there was an insignificant difference between the reduction in water content and the volume shrinkage of the HAp porous green body as a result of drying. Therefore, it can be assumed that only the water contained within the porous body could have evaporated when the samples were maintained in the humid chamber. Thus, a 20% loss of the water from within the porous body during the drying process might further correspond to the 20% shrinkage in sample size, which was observed in Table 3. In Table 2, it can be seen that there is an approximately 20–30% shrinkage in the pore diameter during the course of drying the green HAp porous bodies; additionally, approximately 20% of the observed reduction in the pore diameter occurred during sintering at 1000 °C for 2 h. Thus, the reduction in the pore volume can be calculated using the average of pore diameter. During the course of drying the green HAp porous bodies, there is an approximately 40% shrinkage in the pore volume; furthermore, an approximately 40% shrinkage in the pore volume occurred during sintering at 1000 °C for 2 h. From these results, it is expected that the reduction in the wall space surrounding the pores is lower than that of the pore space. In this study, the sample size was fixed at $5.0 \times 5.0 \times 5.0\ mm^3$ to accommodate the IL treatment. It is possible that a reduction in pore size in addition to a reduction in the sample size may occur due to the small size of the sample.

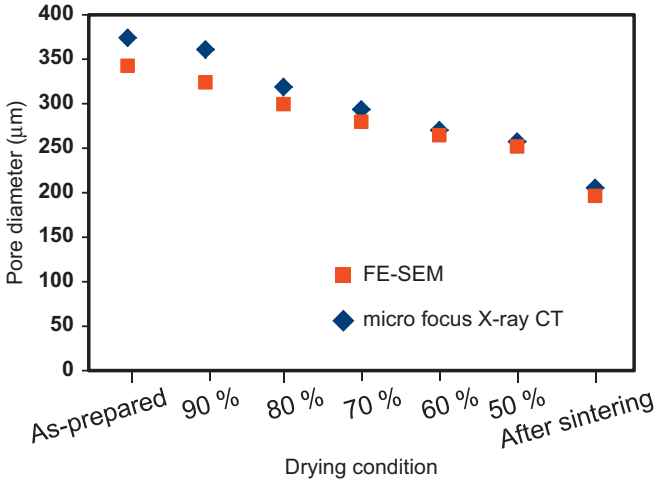

Fig. 9. Distribution of the pore diameters of the HAp green porous body and of the samples maintained in the humid chamber as it was reduced from 90 to 50% relative humidity, as measured from the micro-focused X-ray CT and the FE-SEM images.

In Table 3, it can be seen that, following the IL treatment, the porous HAp body did not show any significant shrinkage even though the porous bodies contained a large amount of water. Therefore, it can be inferred that the hydrophilic IL used in this investigation interacted with the remaining water molecules and that the IL replaced the water within the porous body [27,28]. In our previous study, we reported that the water within the agar gel binds with the IL to form a weak hydrogen bond, thereby preventing the agar gel from dehydrating in the FE-SEM chamber while under vacuum. When the water concentration of the sample following the IL treatment is 30 mol %, the IL and the water molecules have a tendency to form weak hydrogen bonds, such as HOH…BF_4…HOH, in the hydrated porous HAp body. These weak bonds prevent the porous HAp green body from dehydrating in a similar manner to that of the agar gel [35,36], which allows the collection of high-magnification images by FE-SEM. The IL in the present study not only bonds with the water molecules inside the network structures but also acts as a conductive coating, which prevents surface charging of the ceramic bodies like the HAp body investigated in work. To examine the behaviour of the water and the polymer (epoxy resin) used in gelcastings during the drying process, further high-magnification images were collected.

Fig. 10a–f shows the high-magnification FE-SEM images of the as-prepared green HAp porous body and those that were subsequently maintained in the humid chamber. In this study, we focused on the pores of the porous body; due to the wall space, the hydrated specimens proved difficult to cut while maintaining correct morphology. It can be seen that a swollen morphology was observed both in the as-prepared

Table 3
Dimensional changes of the porous HAp green bodies just after removal from the mould and of the samples treated in the humid chamber at 80, 50% relative humidity and of the porous body sintered at 1000 °C for 2 h and examination of the size retention of the green bodies fabricated at a similar condition and subjected to the IL treatment.

Condition	As-preparedwet green body	80%	50%	After sintering, 1000 °C for 2 h
Size retention until sintering (%)	100.0	93.4	78.6	52.7
Size retention after IL treatment (%)	99.0	99.0	99.6	99.8

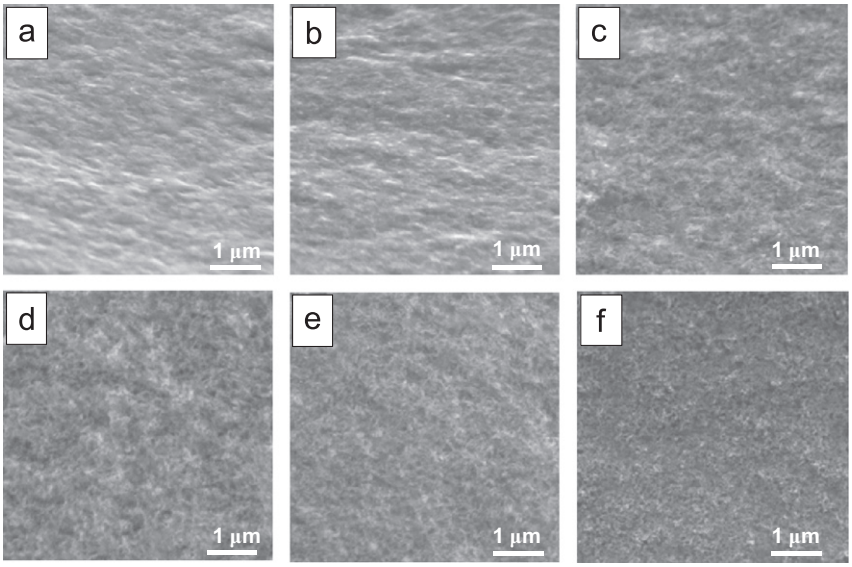

Fig. 10. High-magnification FE-SEM images of (a) the as-prepared porous HAp green body just after removal from the mould and of the samples treated in the humid chamber at (b) 90, (c) 80, (d) 70, (e) 60 and (f) 50% relative humidity.

porous body as well as in the sample maintained in the humid chamber at 90% relative humidity for 1 day (Fig. 10a and b). However, when the relative humidity was decreased from 90 to 50%, due to the gradual loss of the water content, the particles appeared to separate as shown in Fig. 10c–f. The porous bodies maintained in the humid chamber at 50% relative humidity and treated with the IL revealed the presence of fine particles, which were similar in appearance to that of the HAp porous body after sintering (Fig. 10f). Thus, in these FE-SEM images, a fine morphology with sub-micron-sized particles was clearly observed for the specimens treated with the hydrophilic IL or simply maintained in the hydrated conditions.

In this study, the surface morphology of the porous HAp body in its hydrated condition was observed by FE-SEM when the samples were subjected to IL treatment. This simple method of observation can also be applied to a wide range of advanced and traditional ceramics for visual inspection during their wet processing stages. Additionally, other materials, such as wet ceramics, materials interacting with cultured cells and microorganisms, can all be observed by FE-SEM when first subjected to an IL treatment.

4. Conclusions

A simple and convenient method for observing the microstructure of the hydrated porous HAp green body using a hydrophilic IL is reported. The FE-SEM observations showed that the as-prepared porous green body had a pore diameter of approximately 300–600 μm, which gradually decreased to approximately 200–400 μm during drying in a humid chamber from 90 to 50% relative humidity. Wet HAp sample when added into IL, it bonds with water molecules within the HAp–polymer network structure, thereby forming a weak hydrogen bond entangling with the HAp particles surrounding the porous body. This bonding resulted in the formation of an IL–water–HAp–polymer complex, in which the IL acted as a conducting media; additionally, the formation of weak hydrogen bonds between the IL and the water further prevented the porous HAp body from dehydrating in the FE-SEM chamber while under vacuum. Further, the limitations of observing the hydrated porous HAp green body by micro-focused X-ray CT were revealed. It can be concluded from this investigation that it is possible to observe interaction of wet ceramic gels with cultured cell and microorganism using hydrophilic ionic liquid.

References

[1] L.L. Hench, J. Wilson, An Introduction to Bioceramics, World Scientific, Singapore, 1993.
[2] K. de Groot, Clinical applications of calcium phosphate biomaterials: a review, Ceramics International 19 (1993) 363–366.
[3] L.L. Hench, Bioceramics: from concept to clinic, Journal of the American Ceramic Society 74 (1991) 1487–1510.
[4] D.K. Pattanayak, B.T. Rao, T.R. Rama Mohan, Calcium phosphate bioceramics and bioceramic composites, Journal of Sol–Gel Science and Technology 59 (2011) 432–447.
[5] B.S. Chang, C.K. Lee, K.S. Hong, H.J. Youn, H.S. Ryu, S.S. Chung, K.W. Park, Osteoconduction at porous hydroxyapatite with various pore configurations, Biomaterials 21 (2000) 1291–1298.
[6] H. Yuan, K. Kurashina, J.D. de Bruijn, Y. Li, K. de Groot, X. Zhang, A preliminary study on osteoinduction of two kinds of calcium phosphate ceramics, Biomaterials 20 (1999) 1799–1806.
[7] I. Sopyan, M. Mel, S. Ramesh, K.A. Khalid, Porous hydroxyapatite for artificial bone applications, Science and Technology of Advanced Materials 8 (2007) 116–123.
[8] I. Sopyan, J. Kaur, Preparation and characterization of porous hydroxyapatite through polymeric sponge method, Ceramics International 35 (2009) 3161–3168.
[9] S. Padilla, J. Roman, M. Vallet-Regi, Synthesis of porous hydroxyapatite by combination of gelcasting and foams burn out methods,

Journal of Materials Science: Materials in Medicine 13 (2002) 1193–1197.
[10] C.J. Bae, H.W. Kim, Y.H. Koh, H.E. Kim, Hydroxyapatite (HA) bone scaffolds with controlled macrochannel pores, Journal of Materials Science: Materials in Medicine 17 (2006) 517–521.
[11] W.Y. Zhou, S.H. Lee, M. Wang, W.L. Cheung, W.Y. Ip, Selective laser sintering of porous tissue engineering scaffolds from poly (L-lactide)/carbonated hydroxyapatite nanocomposite microspheres, Journal of Materials Science: Materials in Medicine 19 (2008) 2535–2540.
[12] O.O. Omatete, M.A. Janney, R.A. Strehlow, Gelcasting-a new ceramic forming process, American Ceramic Society Bulletin 70 (1991) 1641–1649.
[13] O.O. Omatete, M.A. Janney, S.D. Nunn, Gelcasting: from laboratory development toward industrial production, Journal of the European Ceramic Society 17 (1997) 407–413.
[14] A.C. Young, O.O. Omatete, M.A. Janney, P.A. Menchhofer, Gelcasting of alumina, Journal of the American Ceramic Society 74 (1991) 612–618.
[15] J. Ma, Z. Xie, H. Miao, Y. Huang, Y. Cheng, W. Yang, Gelcasting of alumina ceramics in the mixed acrylamide and polyacrylamide systems, Journal of the European Ceramic Society 23 (2003) 2273–2279.
[16] R.L. Menchavez, M. Fuji, M. Takahashi, Electrically conductive dense and porous alumina with in-situ-synthesized nanoscale carbon networks, Advanced Materials 20 (2008) 2345–2351.
[17] O.O. Omatete, J.P. Pollinger, K. O'Young, Optimization of the gelcasting of a silicon nitride formulation, Ceramic Transactions 56 (1995) 337–343.
[18] L.G. Ma, Y. Huang, J.L. Yang, Z.P. Xie, X.L. Xu, J.S. Zhao, Improving the breakdown strength of rutile capacitor by gelcasting, Journal of Materials Science Letters 20 (2001) 1285–1288.
[19] M.D. Vlajic, V.D. Krstic, Strength and machining of gelcast SiC ceramics, Journal of Materials Science 37 (2002) 2943–2947.
[20] Z.Z. Yi, Z.P. Xie, Y. Huang, J.T. Ma, Y.B. Cheng, Study on gelcasting and properties of recrystallized silicon carbide, Ceramics International 28 (2002) 369–376.
[21] O.O. Omatete, A. Blair, C.G. Westmoreland, A.C. Young, Gelcast zirconia–alumina composites, Ceramic Engineering and Science Proceedings 12 (1991) 2084–2094.
[22] X. Liu, Y. Huang, J. Yang, Effect of rheological properties of the suspension on the mechanical strength of Al_2O_3–ZrO_2 composites prepared by gelcasting, Ceramics International 28 (2002) 59–164.
[23] P. Sepulveda, J.G.P. Binner, S.O. Rogero, O.Z. Higa, J.C. Brsessiani, Production of porous hydroxyapatite by the gelcasting of foams and cytotoxic evaluation, Journal of Biomedical Materials Research 50 (2000) 27–34.
[24] D.J.A. Netz, P. Sepulveda, V.C. Pandolfelli, A.C.C. Spadaro, J.B. Alencastre, M.V.L.B. Bentley, J.M. Marchetti, Potential use of gelcasting hydroxyapatite porous ceramic as an implantable drug delivery system, International Journal of Pharmaceutics 213 (2001) 117–125.
[25] M. Takahashi, K. Adachi, R.L. Menchavez, M. Fuji, Fabrication of semi-conductive ceramics by combination of gelcasting and reduction sintering, Journal of Materials Science 41 (2006) 1965–1972.
[26] C. Hai, J. Liu, H. Watanabe, M. Fuji, F. Wang, M. Takahashi, Surface activation of conductive porous alumina by depositing nickel particles, Journal of the American Ceramic Society 92 (2009) 38–41.
[27] P. Wasserscheid, C.M. Gordon, C. Hilgers, M.J. Muldoon, I.R. Dunkin, Ionic liquids: polar, but weakly coordinating solvents for the first biphasic oligomerisation of ethene to higher [small alpha]-olefins with cationic Ni complexes, Chemical Communications 111 (2001) 1186–1187.
[28] J.F. Wishart, E.W. Castner, The physical chemistry of ionic liquids, Journal of Physical Chemistry B 111 (2007) 4639–4640.
[29] F. Golgovici, A. Cojocaru, L. Anicai, T. Visan, Surface characterization of BiSbTe thermoelectric films electrodeposited from chlorides aqueous solutions and choline chloride based ionic liquids, Materials Chemistry and Physics 126 (2011) 700–706.
[30] T. Torimoto, K. Okazaki, T. Kiyama, K. Hirahara, N. Tanaka, S. Kuwabata, Sputter deposition onto ionic liquids: simple and clean synthesis of highly dispersed ultrafine metal nanoparticles, Applied Physics Letters 89 (2006) 243117.
[31] P. Roy, T. Dey, P. Schmuki, Scanning electron microscopy observation of nanoscopic wetting of TiO_2 nanotubes and ODS modified nanotubes using ionic liquids, Electrochemical and Solid-State Letters 13 (2010) E11–E13.
[32] S. Kuwabata, T. Tsuda, T. Torimoto, Room-temperature ionic liquid as new medium for material production and analyses under vacuum conditions, Journal of Physical Chemistry Letters 1 (2010) 3177–3188.
[33] S. Arimoto, M. Sugimura, H. Kageyama, T. Torimoto, S. Kuwabata, Development of new techniques for scanning electron microscope observation using ionic liquid, Electrochimica Acta 53 (2008) 6228–6234.
[34] K. Kawai, K. Kaneko, H. Kawakami, T. Yonezawa, Bioinspired choline-like ionic liquids: their penetration ability through cell membranes and application to SEM visualization of hydrous samples, Langmuir 27 (2011) 9671–9675.
[35] C. Takahashi, T. Shirai, M. Fuji, Electron microscopic observation of fine morphology of wet agar gel using a typical hydrophilic ionic liquid; 1-butyl-3-methylimidazolium tetrafluoroborate, Advances in Technology of Materials Processing Journal 13 (2011) 39–47.
[36] C. Takahashi, T. Shirai, M. Fuji, Observation of interactions between hydrophilic ionic liquid and water on wet agar gels by FE-SEM and its mechanism, Materials Chemistry and Physics 133 (2012) 565–572.
[37] D. Oyamatsu, T. Fujita, S. Arimoto, H. Munakata, H. Matsumoto, S. Kuwabata, Electrochemical desorption of a self-assembled monolayer of alkanethiol in ionic liquids, Journal of Electroanalytical Chemistry 615 (2008) 110–116.